Performance operation of liquid ejectors for a R744 integrated multi-ejector supermarket system using a hybrid ROM

Michal Haida[a,*], Jacek Smolka[a], Armin Hafner[b], Michal Palacz[a], Ziemowit Ostrowski[a], Jakub Bodys[a], Ekaterini K. Kriezi[c], Sven Försterling[d], Andrzej J. Nowak[a], Krzysztof Banasiak[e]

[a] *Institute of Thermal Technology, Silesian University of Technology, Konarskiego 22, 44-100 Gliwice, Poland*
[b] *NTNU Department of Energy and Process Engineering, Kolbjørn Hejes vei 1d, 7465 Trondheim, Norway*
[c] *Danfoss Company, Denmark*
[d] *TLK-Thermo GmbH, 38106 Braunschweig, Germany*
[e] *SINTEF Energy, Kolbjørn Hejes vei 1d, 7465 Trondheim, Norway*

Abstract

Performance maps were generated for designed liquid ejectors installed in a multi-ejector module in an R744 integrated supermarket system using a hybrid of the reduced-order model (ROM). Hybrid ROMs of the investigated liquid ejectors were developed based on experimental data and CFD results. The CFD model achieved satisfactory accuracy at motive nozzle pressures above 59 bar, and the hybrid ROM improved the mass flow rate prediction. Maps were generated for the motive nozzle mass flow rate and the mass entrainment ratio at different ambient conditions related to cold, moderate, and hot climate zones. The set of the pressure lift for ejector efficiency maximisation at different ambient conditions is presented for refrigeration and air-conditioning applications. The developed liquid ejectors hybrid ROMs can be used to optimise work of the R744 integrated supermarket system equipped with the vapour and liquid ejectors.

Keywords: carbon dioxide, refrigeration system, liquid ejector, reduced-order model, CFD model

1. Introduction

Natural refrigerants, especially carbon dioxide (denoted as R744), have been more and more often used in commercial applications due to the restrictive regulations regarding refrigerant selection, i.e., Kigali Anmenmend (United Nations, 2017) or European Union F-gas regulation (European Parliament and Council of EU, 2014). According to Gullo et al. (2018a), the favourable thermal properties of the carbon dioxide (CO_2) led to define the transcritical CO_2 systems as a standard for the commercial refrigeration sector. However, high thermodynamic losses during system operation in transcritical mode required to improve the system coefficient of performance (COP) of the R744 refrigeration system. One of the solutions is to integrate different applications into an "all-in-one" CO_2 cooling system (Pardiñas et al., 2018).

* Tel.: +48 322372810; Michal.Haida@polsl.pl

The integration of refrigeration and air-conditioning applications has occurred in supermarkets (Purohit et al., 2018). Moreover, the systems were designed as transcritical booster systems with parallel compression for energy performance improvements. Sharma et al. (2014) compared different configurations of the R744 refrigeration system with the R410A direct expansion system based on annual work in different regions of the United States. The authors stated that the R744 booster system with parallel compression obtained a similar COP as the R410A system, especially in hot climates. Sooben et al. (2019) performed case study analysis of the R744 transcritical supermarket systems and HCFC's and HFC's systems in Mauritius. According to authors conclusions, a 5.6% reduction in energy consumption was reached for the R744 parallel compression system when compared to the baseline system.

The COP improvement can be achieved by using the evaporators in the flooded mode (Minetto et al., 2014), which allows the evaporators to increase the evaporation temperature and reduce the pressure ratio in the compressor section. However, the liquid phase of the refrigerant appeared in the evaporator outlet must be recirculated to avoid liquid injection into the compressors. The recirculation of the liquid stream can be performed using liquid ejectors combined with vapour ejectors that are also used as main expansion devices (Hafner et al., 2014).

The main purpose of the liquid ejectors is to pump the liquid R744 stream from the evaporator or from the suction accumulator tank due to the expanded motive stream from the gas cooler outlet (Sumeru et al., 2012). The motive high-pressure flow is expanded in the converging-diverging nozzle, and supersonic conditions are reached immediately after the throat. Therefore, the supersonic flow can entrain the suction flow from the suction nozzle in the mixing section. The high kinetic energy of the mixed stream is replaced into pressure energy in the diffuser. Hence, the stream outside the ejector enters the intermediate-pressure liquid receiver due to the higher pressure at the outlet when compared to the suction nozzle. The liquid ejector possibility to pump the suction liquid flow from the flooded evaporators let to improve the COP of the ejector-based refrigeration system. Moreover, integration with the vapour ejectors, which are used as main expansion devices to entrain vapour flow from the evaporator, allows efficient control over the system work at different cooling capacities and ambient temperatures (Hafner et al., 2014).

Theoretical and experimental analysis of an R744 refrigeration system equipped with a liquid ejector confirmed the COP improvement of the system with flooded evaporators. Minetto et al. (2014) carried out experimental tests of a parallel compression refrigeration system with liquid re-circulating flooded evaporators. The liquid flow from the evaporator was pumped by a two-phase ejector. The authors stated that the electric power consumption was reduced up to 13% compared to the standard configuration. Hafner et al. (2014) presented a multi-ejector concept equipped with fixed-type vapour and liquid ejectors designed to cover supermarket capacities in different climate zones. According to dynamic simulations, the COP improvement of the R744 multi-ejector refrigeration system increased to 30%. Purohit et al. (2018) performed a theoretical comparison of different configurations of the R744 integrated supermarket system. The authors stated that implementation of the liquid and vapour ejectors improved the operation in cold, moderate, and mildly warm climates. Gullo et al. (2018b) defined the potential boundary line of efficient utilisation of the R744 multi-ejector system below Northern Africa. Hence, the optimum control strategy of the R744 integrated system and design process of the ejector to obtain the best efficiency allows further COP improvements and increases the competitiveness of the R744 integrated system. However, complex phenomena occurred inside the two-phase ejector which forced the use of more advanced mathematical approaches to predict the ejector performance at a wide operating regime to design the shape for optimum efficiency.

The performance of the liquid ejector was evaluated by numerical approaches, specifically by computational fluid dynamics (CFD). Zaheer and Masud (2017) compared Reynolds-Averaged Navier-Stokes (RANS) turbulent models with the Large Eddy Simulation turbulent approach for liquid ejectors used in aircraft fuel systems. The characteristics of fluid flow parameters, i.e., pressure and velocity, were compared with the experimental data. According to Zaheer and Masud (2017), the LES approach provided more detailed information about flow instabilities inside the ejector, along with the cost of the computational time. Ismagilov et al. (2017) investigated nozzle reduction using a blade agitator on the liquid jet ejector efficiency to define the optimum nozzle throat area. Haida et al. (2016b) numerically analysed R744 liquid ejectors installed in a prototype multi-ejector module. The homogeneous equilibrium fluid (HEM) flow assumption was used in the enthalpy-based energy formulation CFD model developed by Smolka et al. (2013) and validated by Palacz et al. (2015). Moreover, the crucial geometry procedure was parameterized to determine the potential improvement in the liquid ejector performance. According

to Haida et al. (2016b), the best performance was obtained at short pre-mixer and mixer lengths compared to the liquid ejectors installed in the prototype module. Moreover, the validation procedure confirmed the need to use a more complex two-phase fluid flow assumption to improve the CFD model accuracy.

The numerical investigations of the liquid ejector defined possible performance improvement by shape modification at the defined operating regimes. However, the control strategy of the R744 integrated supermarket system equipped with liquid ejectors maintained optimum COP during system operation. Theoretical and dynamic simulations were performed based on the non-dimensional or one-dimensional mathematical approach of the two-phase ejector to evaluate the performance of the liquid ejector installed in the refrigeration and air-conditioning cycles. One of the aforementioned models was developed by Kornhauser (1990), which assumed the efficiency of each ejector part and the pressure level inside the mixing section. Lawrence and Elbel (2018) used the Kornhauser model to investigate the numerical energy performance of a microchannel evaporator design integrated with a two-phase ejector used either as a liquid ejector or a vapour ejector. A performance analysis was done for R744 and R410A, and the authors concluded that the liquid ejector should be operated to avoid a large amount of evaporator flooding.

The simplified ejector model allowed the ejector work to be evaluated in a short computational time but with a low accuracy of the real performance predictions. On the other hand, the CFD model could not be implemented in the system simulations due to the computational time costs. One of the solutions is to implement the low-order, fast, and accurate models, such as the reduced-order model (ROM) that can be used in the dynamic simulations of the R744 integrated system for best performance. Haida et al. (2018b) developed the ROM for the R744 vapour ejector based on the CFD results. For sake of completeness, this is repeated here as follows: "The proper orthogonal decomposition model with radial basis interpolation functions (POD-RBF) was employed for ejector performance evaluation at arbitrary operating conditions. The low-order approach obtained a similar accuracy to the CFD model compared to the experimental data". Even higher accuracy was obtained by the ROM model that was defined based on the hybrid combination of the experimental data and CFD results. This was used to build a performance maps of designed vapour ejectors installed in the multi-ejector module at the HVAC&R operating regime (Haida et al., 2018a). The authors wrote as follows: "The best efficiency area of each vapour ejector was defined for areas close to the critical point and at very high-pressure lifts, especially for air-conditioning applications. Moreover, the hybrid ROMs of the vapour ejector were successfully integrated into the commercial software for system dynamic simulations and component selection".

The main benefit of adding a liquid ejector to the R744 integrated system is the ability to recirculate liquid flow from the evaporator section. The different flow behaviour and application of the liquid ejectors in the refrigeration system required development of the fast and accurate numerical model. Theoretical and numerical analyses of the liquid ejectors found in the literature have confirmed the necessity to utilise liquid ejectors to improve COP, however, a more thorough investigation is required to evaluate their performance and maximise their entrainment prospects. Therefore, the main aim of this paper is to perform a numerical investigation and performance mapping of the designed liquid ejectors for a R744 integrated supermarket system. First, a validation procedure of the CFD model with the implemented modified HRM approach was performed to calibrate the numerical model. Then, the hybrid ROM of the liquid ejectors was developed based on the experimental data obtained from the test rig located in the SINTEF Energy Research laboratory in Trondheim and the results from the validated CFD model. Then, the motive nozzle mass flow rate (MFR) and the mass entrainment ratio (MER) maps were generated for each liquid ejector at a wide range of operating conditions. Finally, a set of the pressure lift ranges for ejector efficiency maximisation is presented at typical operating conditions for supermarket refrigeration and air-conditioning applications. The developed hybrid ROM can be further used to optimise the R744 integrated supermarket system energy performance equipped with the vapour and liquid ejectors due to the implementation of each hybrid ROM to dynamic simulations of the aforementioned system. In order to perform performance operation analysis of R744 liquid ejectors, the following information was taken from authors previous work:

- the R744 vapour compression test rig presented by Banasiak et al. (2015) and Haida et al. (2016a),
- the CFD modified HRM approach proposed for R744 vapour ejector by Haida et al. (2018c),
- the POD-RBF approach developed for R744 vapour ejector from Haida et al. (2018b).

2. The R744 multi-ejector module equipped with liquid ejectors

The R744 integrated supermarket system equipped with the multi-ejector model covered varying cooling demands due to the use of ejectors in single and parallel modes. The schema of the module with inlet and outlet ports that contains six fixed-geometry ejectors was shown in Figure 1. The first two ejectors named LEJ1 and LEJ2 were designed to recirculate liquid flow from the evaporator section, and the remaining ejectors were designed as vapour ejectors for partial re-compression. In addition, the control system connected with the solenoid valves allowed the ejectors to be used in either single or parallel operation. The multi-ejector module was described in details by Banasiak et al. (2015). The main dimensions of both liquid ejectors are provided in Table 1. The motive nozzle of each liquid ejector was designed as a converging nozzle. Hence, the sonic conditions were reached at the end of the motive nozzle part.

Table 1: The main geometry parameters of the liquid ejectors installed in the R744 multi-ejector module.

Parameter name	Unit	LEJ 1	LEJ 2
Motive nozzle inlet diameter	10^{-3} m	3.80	3.80
Motive nozzle throat diameter	10^{-3} m	1.21	1.71
Motive nozzle converging angle	°	30.00	30.00
Diffuser outlet diameter	10^{-3} m	7.30	8.40
Diffuser angle	°	5.00	5.00

Figure 2 presents the operating regime for the motive nozzle of both liquid ejectors considered in this investigation. As shown in Figure 2, the motive nozzle pressure was defined in the range from 50 bar to 140 bar to analyse the ejector performance at various ambient temperatures defined for cold, moderate, hot, and tropical climate zones. In addition, the motive nozzle specific enthalpy was defined between the saturated liquid and up to 340 kJ·kg^{-1} in the transcritical region and with different subcooling degree related to the temperature in the range from 5 °C to 55 °C. The defined motive nozzle operating regime of the liquid ejectors was similar to the motive nozzle regime specified for the vapour ejectors due to the operation of the multi-ejector module in the supermarket refrigeration system (Haida et al., 2018a).

The suction nozzle and outlet operating conditions, together with the motive nozzle conditions, are presented in Table 2. The suction nozzle operating conditions between 26 bar and 46 bar were defined to analyse the ejector performance for saturated liquid. Moreover, the suction nozzle operating regime was related to the different applications appeared in the integrated supermarket system similar to work presented by Haida et al. (2018a). The outlet conditions were defined by the outlet pressure to evaluate ejector work at pressure difference between outlet and suction nozzle in the range from 3 bar and 10 bar. Hence, the lowest outlet pressure was 29 bar, and the highest was 56 bar.

Table 2: The motive nozzle, the suction nozzle, and outlet operating conditions of investigated liquid ejectors.

Boundary condition	Motive nozzle		Suction nozzle		Outlet
Parameter	Pressure	Temperature	Pressure	Temperature	Pressure
Unit	bar	°C	bar	°C	bar
Min	50	15	26	-10.65	29
Max	140	60	46	10.87	56

The performance mapping at the wide operating range has to be done by the use of a complex mathematical model, such as a CFD approach, to predict MFRs through both nozzles for each ejector. Therefore, the CFD model

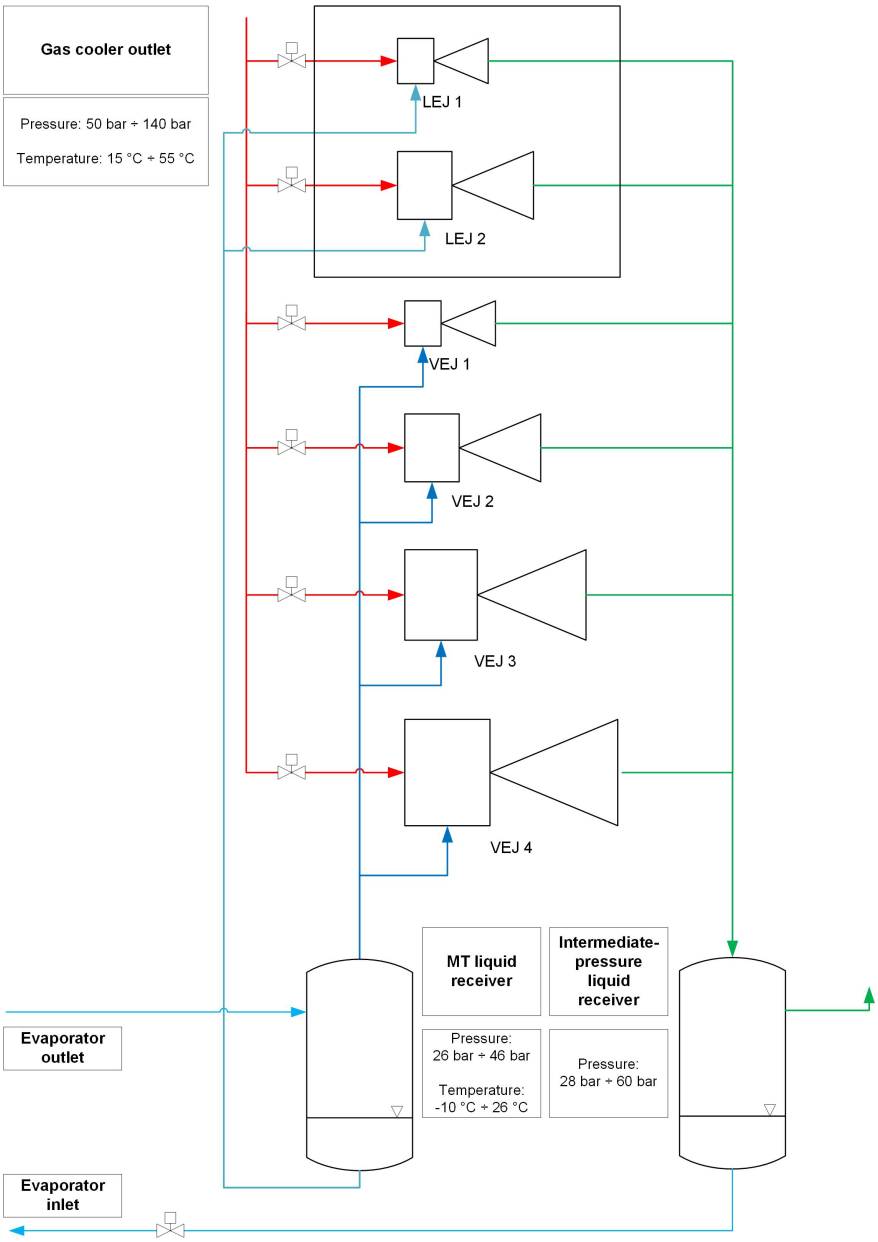

Figure 1: The layout of the R744 multi-ejector module adapted and modified from Haida et al. (2018a).

with the modified HRM was used to simulate R744 flow behaviour inside the liquid ejector. Moreover, the results obtained from the CFD model were compared with the experimental data to define the range of the numerical model application.

3. Experimental test campaign

In this section, the experimental investigation of the R744 liquid ejectors is described. The test facility equipped with the CTM-6 multi-ejector module is presented in Section 3.1. Then, the sensor specifications used in the R744 multi-ejector test rig is shown together with the test series description in Section 3.2. Finally, the experimental data obtained during the experimental investigation are presented in Section 3.3.

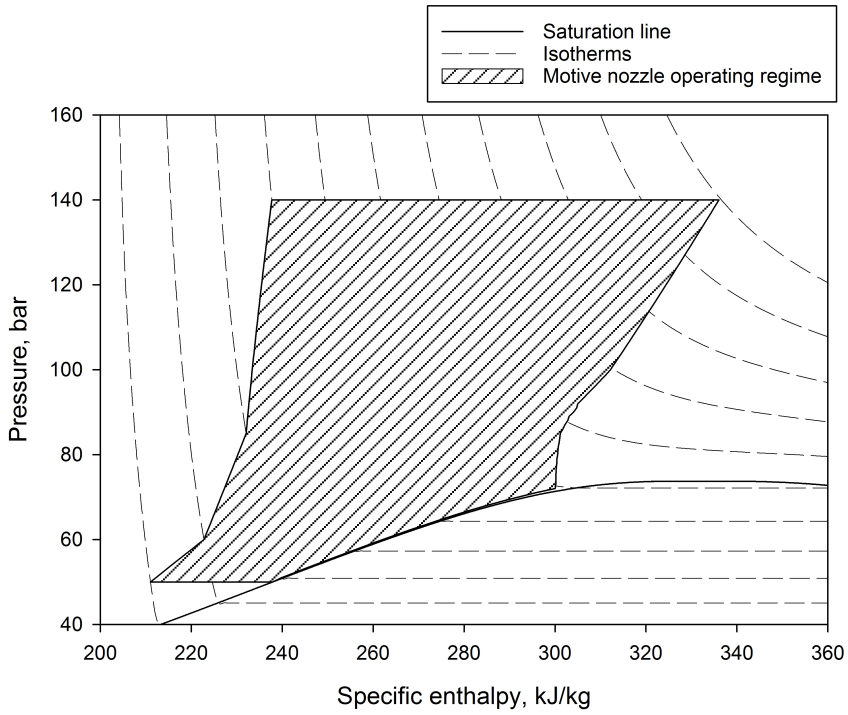

Figure 2: A pressure-specific enthalpy diagram with the motive nozzle operating regime of each R744 liquid ejector adapted from Haida et al. (2018a).

3.1. Test facility

Figure 3 presents the test facility used for experimental investigation of liquid ejectors. The test rig was designed as the R744 vapour compression rack with parallel compression and presented by Haida et al. (2016a) for vapour ejectors experiments. Two parallel compressors and MT compressor manufactured by Dorin were connected to inverters for continuous work regulation. The gas cooler section was divided into two brazed plate-typed heat exchangers to control the gas cooler outlet temperature due to the heat absorption by the glycol loops. The internal heat exchanger was used to define different subcooling degree and to avoid the liquid droplets inside the compressor. The expansion process is done by the high-electronic expansion valve (HPV in Figure 3) and partially by liquid ejectors installed in the multi-ejector either in single mode or in parallel mode. The liquid receiver and suction accumulator were used to provide the liquid flow in the evaporator and liquid ejectors. The MT evaporator was utilised in a flooded mode due to the heat rejection by the additional glycol loop and the two-phase stream is entered to the suction accumulator tank.

The liquid ejectors were utilised to compress the liquid flow from the suction accumulator and expanded the high-side pressure from internal heat exchanger outlet. The ejectors installed in the multi-ejector module were operated by the solenoid valves located before the motive nozzle of each ejector. The suction collector of the liquid ejectors was connected to the bottom side of the suction accumulator to ensure the liquid phase of the entrained flow. The outlet flow from the liquid ejectors entered to the liquid receiver. Hence, the liquid flow from the evaporator was recirculated during the liquid ejectors work.

3.2. Measurements and control system

In Table 3, all sensors used to measure system parameters and liquid ejectors performances are listed. Moreover, the accuracy of each measurement was presented together with the data range. The test facility was fully-equipped with the sensors to measure flow parameters, such as the pressure, temperature and mass flow rate. In Haida et al. (2016a) the authors already described the measurements of the test rig. For sake of completeness, this is repeated as follows: "The temperature was measured by a PT1000 resistance thermometer. An accuracy of the

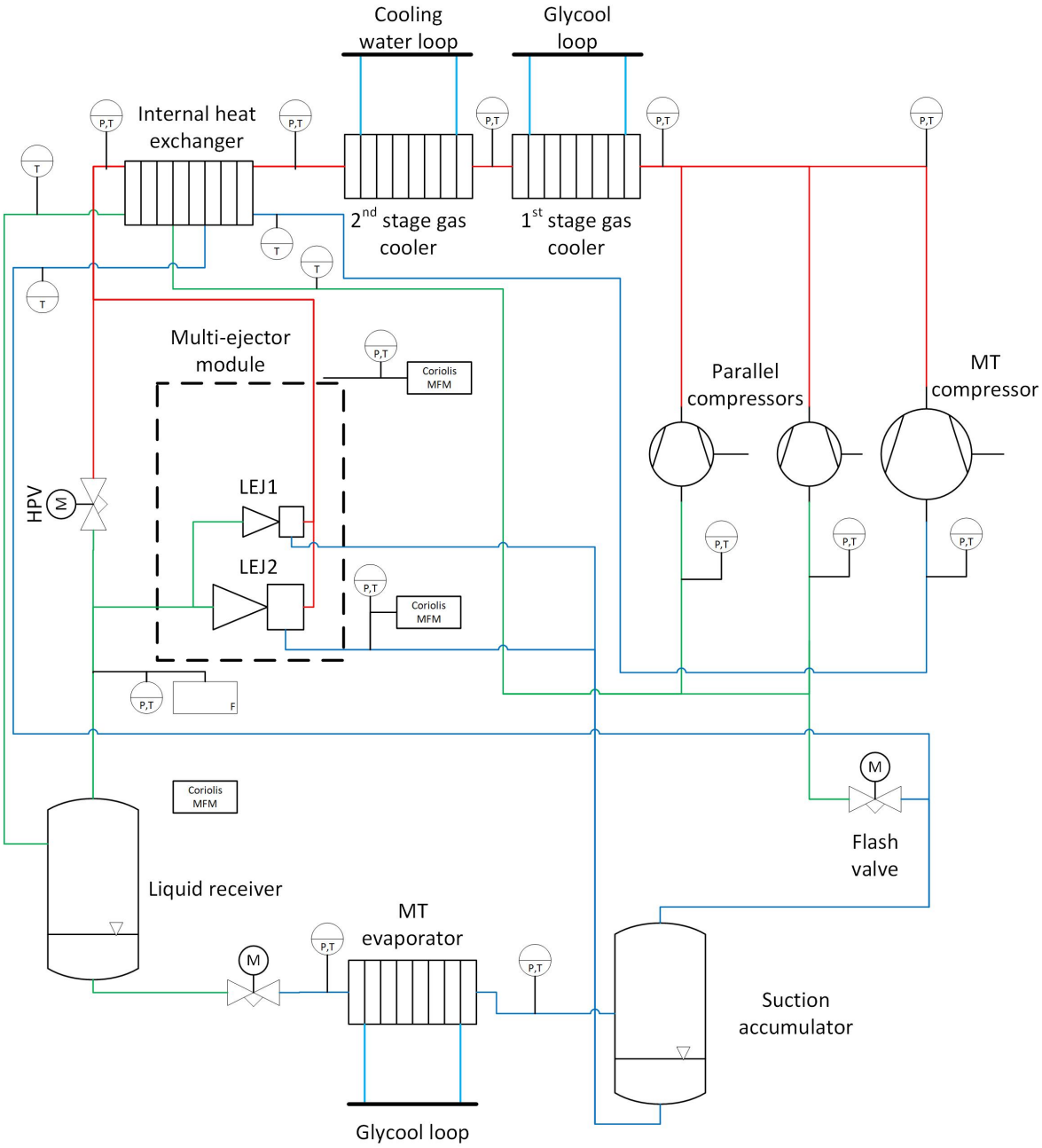

Figure 3: The R744 vapour compression test rig equipped with two liquid ejectors in the multi-ejector module adapted and modified from Haida et al. (2016a).

temperature measurement was of $\pm(0.3 + 0.005\ t)$, where t is the temperature in °C. The pressure was measured using a piezoelectric transmitter with an accuracy of ±0.3%. Finally, Coriolis-type RHM06 and RHM15 transducers were used for mass flow rate measurements, with an accuracy of ±0.2%. All sensors were connected with a Danfoss control unit. Moreover, the aforementioned measurements were also located at the inlet and outlet ports of the multi-ejector module". Additional details about the test facility are reported in the work of Haida et al. (2016a).

The test campaign was carried out to obtain a set of different operating conditions under subcritical and tran-

Table 3: The set of the instrumentations used for experimental investigation of liquid ejectors.

Parameter	Sensor	Accuracy	Data range
Temperature	Resistance thermometer PT1000	$\pm(0.3 + 0.005\ t)$	-70 °C÷180 °C
Pressure	Piezoelectric transmitter	±0.3% of reading	0÷100 bar and 0÷150 bar
Mass flow rate	Coriolis-type RHM06	±0.2% of reading	0÷20 kg min^{-1}
Mass flow rate	Coriolis-type RHM15	±0.2% of reading	0÷200 kg min^{-1}

scritical conditions. The required boundary conditions were defined by a set of the gas cooler outlet pressure and temperature, the liquid receiver pressure and the evaporator pressure. Each operating point was reached when all parameters defining ejector performance such as the motive nozzle pressure, temperature and mass flow rate, suction nozzle pressure and mass flow rate and outlet pressure were constant or with small deviation within the period longer than 10 minutes. The recorded signals from measurements were processed and transferred by Danfoss Minilog data acquisition system with the record interval of 5 second. Hence, the data for single operating point were calculated based on the uncertainty analysis.

3.3. Experimental data

The experimental investigation was done to evaluate ejector performance of two liquid ejectors utilised in a single mode. The work of each ejector was analysed based on the pressure lift, MER and the ejector efficiency parameters. Moreover, the experimental data presented in this section were selected for the validation procedure of the modified HRM CFD model.

Figure 4 presents the operating points selected for the validation procedure of the modified HRM CFD model. The MN conditions for the smaller liquid ejector LEJ1 are shown on the pressure-specific enthalpy diagram in Figure 4(a). The operating conditions were selected to evaluate the mass flow rate prediction of the CFD model in the subcritical region, close to the critical point, and in the transcritical region. Different degrees of subcooling were achieved during experiments at MN pressures from approximately 50 bar to almost 100 bar, and similar MN conditions were chosen for the larger liquid ejector LEJ2, which is shown in Figure 4(b). The selected points for both liquid ejectors were defined in terms of different pressure lifts below 4 bar, between 4 and 8 bar, and above 8 bar. Hence, Figure 4(c) presents the pressure lift in terms of the SN pressure for each ejector and shows that the SN pressure varied from approximately 26 bar to almost 34 bar, which is typical for refrigeration applications. A maximum pressure lift of 12 bar was obtained by LEJ2 and approximately 11.5 bar by LEJ1 for an SN pressure of approximately 32 bar.

Table 4 presents the set of the experimental data and performance parameters of the smaller liquid ejector LEJ1 used for the validation procedure. The pressure lift varied from 2.7 bar to over 11.0 bar, which strongly related to MER and the ejector efficiency. The lowest pressure lift was reached for L1_25 at the subcritical conditions and the suction nozzle pressure of approximately 33.0 bar. The highest pressure lift of 11.2 bar was obtained for L1_11 at the motive pressure of approximately 80.0 bar and the suction nozzle pressure of approximately 32.0 bar. According to the motive nozzle conditions and pressure lift values, MER was in the range from 0.09 for L1_30 at the motive nozzle pressure of approximately 55.0 bar to 0.90 for L1_7 at the transcritical region above 87.0 bar. Both parameters allows for the recirculation of suction liquid stream at different flooded evaporator working pressure and recover some potential expansion work. The liquid ejector utilised at possible highest MER at high pressure lift ensure the liquid level reduction in the suction accumulator and the pressure ratio reduction in the parallel compressors.

Another parameter describing ejector performance is the ejector efficiency, which combines aforementioned pressure lift and MER. The liquid ejector LEJ1 obtained ejector efficiency in the range from over 0.7% to almost 10.0%. At the transcritical conditions, the highest efficiency of 9.64% was reached for L1_14 at the pressure lift of almost 9.0 bar and MER of 0.67. The highest efficiency of LEJ1 was of 8.58% below the critical point for L1_26 due to the pressure lift of 6.1 bar and maintained high value of MER of 0.66.

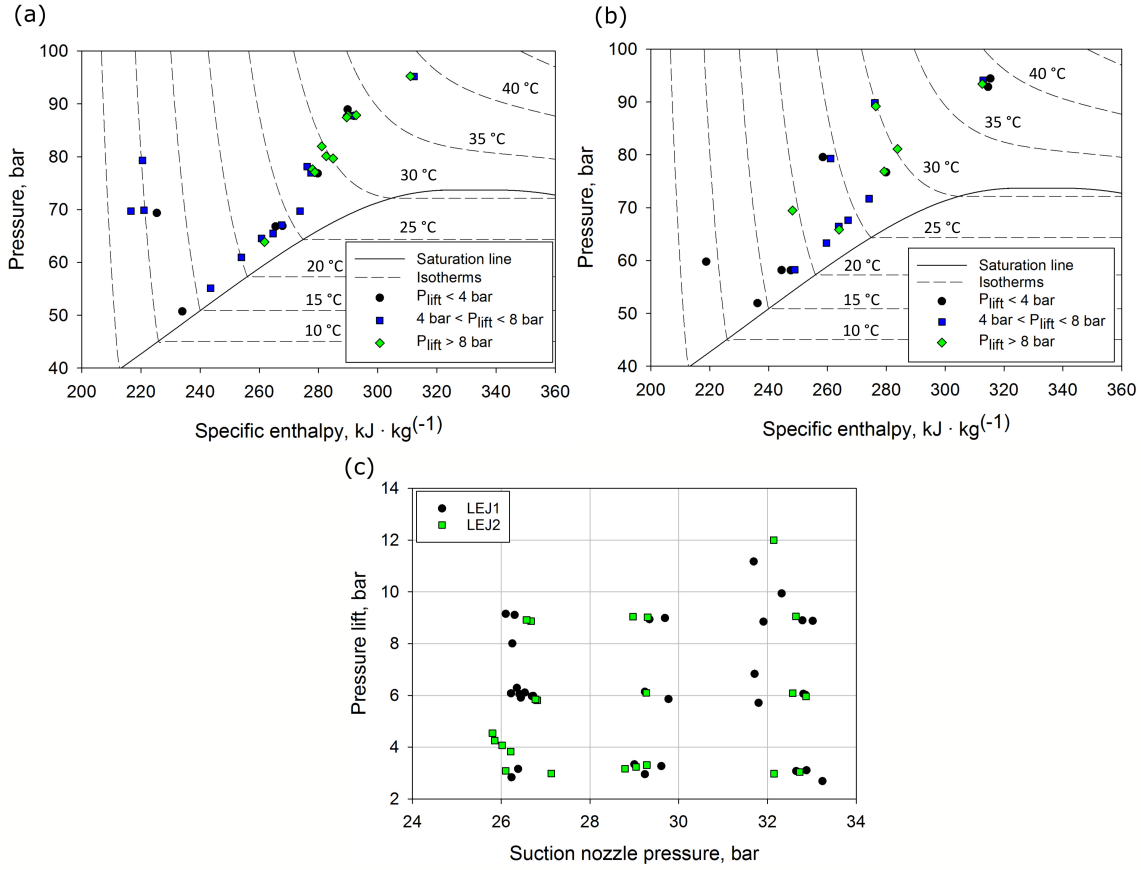

Figure 4: The operating conditions selected for the validation procedure: (a) the R744 p-h diagram with LEJ1 MN conditions; (b) the R744 p-h diagram with LEJ2 MN conditions; (c) the pressure lift in terms of the suction nozzle pressure for both liquid ejectors.

Similar to the results presented in Table 4, the set of the experimental data together with the performance parameters of LEJ2 was listed in Table 5. The pressure lift was in the range from 3.0 bar up to 12.0 bar and the highest pressure lift was reached for L2_7 at the motive nozzle pressure above 80.0 bar and the suction nozzle of approximately 32.0 bar. In addition, LEJ2 obtained higher MER range for investigated experimental points from 0.16 to 0.95. The combination of high MER and high pressure lift indicated the ejector efficiency above 10% for L2_7 and L2_10. At the subcritical conditions, the highest efficiency of approximately 8.6% was obtained for L2_19 at the motive nozzle pressure of approximately 60.0 bar due to the pressure lift of approximately 6.0 bar and MER of 0.44.

The experimental data of investigated liquid ejectors confirmed high entrainment possibility at the pressure lift up to 12.0 bar. However, the ejector efficiency was below 15% for all investigated points. As a comparison, the vapour ejectors analysed by Banasiak et al. (2015) obtained ejector efficiency up to 30% due to the entrainment of the superheated vapour stream from the evaporator. However, the performance mapping of the liquid ejectors allows for the improvement of the ejector efficiency maintaining high liquid flow recirculation from the flooded evaporators. The maps generation of the liquid ejectors can be done using fast and accurate ROM based on the validated CFD model combined with the experimental data of designed ejectors.

Table 4: The set of the experimental data of the R744 liquid ejector LEJ1.

OC	Experimental data						Performance parameters		
	P_{MN}	T_{MN}	P_{SN}	P_{out}	$\dot{m}_{MN}$	$\dot{m}_{SN}$	P_{lift}	χ	η_{ej}
	bar	K	bar	bar	kg·min^{-1}	kg·min^{-1}	bar	-	%
L1_1	95.2	311.5	29.3	38.3	3.01	2.35	9.00	0.78	5.51
L1_2	95.2	311.7	29.2	35.4	2.98	2.38	6.20	0.80	3.49
L1_3	88.9	306.2	26.2	29.1	3.35	1.89	2.90	0.56	1.17
L1_4	87.9	306.5	32.8	41.7	3.10	2.57	8.90	0.83	8.62
L1_5	87.8	305.9	29.7	38.7	3.29	2.19	9.00	0.67	6.31
L1_6	87.8	306.1	26.4	32.5	3.18	1.94	6.10	0.61	3.02
L1_7	87.7	306.3	32.7	35.7	3.16	2.83	3.00	0.90	2.54
L1_8	87.5	305.8	26.1	35.3	3.21	1.80	9.20	0.56	4.70
L1_9	82.0	302.9	32.3	42.3	3.30	2.05	10.00	0.62	9.15
L1_10	80.1	302.9	31.9	40.8	3.12	2.29	8.90	0.73	9.15
L1_11	79.7	303.2	31.7	42.9	2.97	1.39	11.20	0.47	7.92
L1_12	79.3	283.3	26.5	32.6	6.21	2.72	6.10	0.44	4.89
L1_13	78.1	301.2	29.8	35.6	3.37	2.23	5.80	0.66	4.69
L1_14	77.6	301.5	33.0	41.9	3.23	2.15	8.90	0.67	9.64
L1_15	77.3	301.4	32.9	36.0	3.25	2.77	3.10	0.85	3.34
L1_16	77.1	301.5	26.3	35.4	3.02	1.71	9.10	0.57	6.03
L1_17	76.9	301.2	32.9	38.9	3.19	2.68	6.00	0.84	7.32
L1_18	76.8	301.7	29.2	32.2	2.99	2.53	3.00	0.85	2.62
L1_19	69.9	283.0	26.7	32.7	5.58	2.54	6.00	0.46	6.11
L1_20	69.7	281.3	26.4	32.6	5.68	2.66	6.20	0.47	6.75
L1_21	69.7	299.1	26.4	32.4	3.18	1.50	6.00	0.47	3.40
L1_22	69.4	284.7	26.4	29.5	5.50	2.59	3.10	0.47	2.71
L1_23	67.1	297.3	26.2	32.3	3.78	0.34	6.10	0.09	0.73
L1_24	66.9	297.4	29.6	32.9	3.35	2.18	3.30	0.65	3.02
L1_25	66.8	296.8	33.2	35.9	3.37	2.64	2.70	0.78	3.70
L1_26	65.5	296.4	32.8	38.9	3.31	2.17	6.10	0.66	8.58
L1_27	64.5	295.4	26.7	32.7	3.46	1.54	6.00	0.45	4.15
L1_28	63.9	295.5	26.2	34.3	3.40	0.56	8.10	0.16	2.26
L1_29	60.9	293.2	31.7	38.5	3.31	0.47	6.80	0.14	2.63
L1_30	55.1	289.6	31.8	37.5	3.58	0.34	5.70	0.09	1.98
L1_31	50.7	286.3	29.0	32.3	3.83	2.04	3.30	0.53	5.70

4. The liquid ejector CFD model

In this section, the CFD model of the R744 liquid ejector is described. The modified HRM was previously described by Haida et al. (2018c) for a R744 two-phase ejector, and the enthalpy-based energy equation formulation was applied by Smolka et al. (2013). For sake of completeness, this is repeated here as follows: "A modified homogeneous relaxation approach was used to evaluate the flow behaviour inside the ejector considering the flow metastability. The metastable effect of the R744 flow inside the ejector is considered in HRM by the additional vapour mass balance governing equation". In addition, the relaxation time was defined for different motive nozzle conditions below 59 bar, below the critical point, and at transcritical conditions to evaluate the influence of the flow metastability on the expansion process and ejector performance.

Table 5: The set of the experimental data of the R744 liquid ejector LEJ2.

OC	Experimental data						Performance parameters		
	P_{MN}	T_{MN}	P_{SN}	P_{out}	$\dot{m}_{MN}$	$\dot{m}_{SN}$	P_{lift}	χ	η_{ej}
	bar	K	bar	bar	kg·min^{-1}	kg·min^{-1}	bar	-	%
L2_1	94.5	311.9	32.1	35.1	5.71	5.42	3.00	0.95	2.00
L2_2	94.1	311.5	32.6	38.7	5.80	5.35	6.10	0.92	4.55
L2_3	93.4	311.2	29.0	38.0	5.82	4.50	9.00	0.77	5.43
L2_4	92.9	311.4	29.0	32.3	5.69	4.61	3.30	0.81	1.70
L2_5	89.8	303.1	26.8	32.6	8.32	2.32	5.80	0.28	1.49
L2_6	89.2	303.1	26.6	35.5	8.08	2.41	8.90	0.30	2.72
L2_7	81.1	303.3	32.1	44.1	6.02	3.29	12.00	0.55	10.28
L2_8	79.6	296.8	27.1	30.1	9.05	1.77	3.00	0.20	0.66
L2_9	79.3	297.5	26.8	32.6	8.90	1.65	5.80	0.19	1.31
L2_10	76.9	301.6	32.6	41.7	5.96	4.73	9.10	0.79	11.62
L2_11	76.7	301.7	28.8	32.0	5.73	4.80	3.20	0.84	2.73
L2_12	71.7	299.6	25.8	30.3	6.38	3.40	4.50	0.53	2.51
L2_13	69.5	292.5	26.7	35.5	9.05	1.48	8.80	0.16	2.76
L2_14	67.7	297.3	25.8	30.1	6.55	3.11	4.30	0.47	2.43
L2_15	66.4	296.4	29.3	35.4	6.30	4.05	6.10	0.64	6.67
L2_16	65.9	296.3	29.3	38.3	6.49	2.18	9.00	0.34	6.11
L2_17	63.3	294.9	26.0	30.1	6.73	2.77	4.10	0.41	2.35
L2_18	59.8	281.6	26.1	29.2	9.77	4.64	3.10	0.47	3.61
L2_19	58.3	291.5	32.9	38.8	7.40	3.26	5.90	0.44	8.58
L2_20	58.2	290.2	26.2	30.0	7.98	1.63	3.80	0.20	1.45
L2_21	58.1	291.1	32.7	35.8	7.97	3.77	3.10	0.47	4.01
L2_22	51.9	287.1	29.3	32.6	7.71	4.22	3.30	0.55	5.55

4.1. *EjectorPL platform*

The automation of the geometry and mesh preparation, together with the CFD calculation and post-processing, was performed by developing the *ejectorPL* platform (Palacz et al., 2015). This platform has been successfully used in several numerical investigations involving CO_2 ejectors, including the parametrisation procedure of R744 liquid ejectors (Haida et al., 2016b) and shape optimisation of the R744 two-phase ejector (Palacz et al., 2017). The simulation strategy flowchart is shown in Figure 5, which shows that the post-processing obtained both local and global results, i.e., mass flow rates, temperature, and flow variable contours, or single vector (called *snapshot*) that can be implemented to ROM (Haida et al., 2018b). Moreover, the coupled heat transfer with the two-phase flow model can be calculated to evaluate the heat conduction in ejector walls, but the ejector walls were defined as an adiabatic wall in this paper.

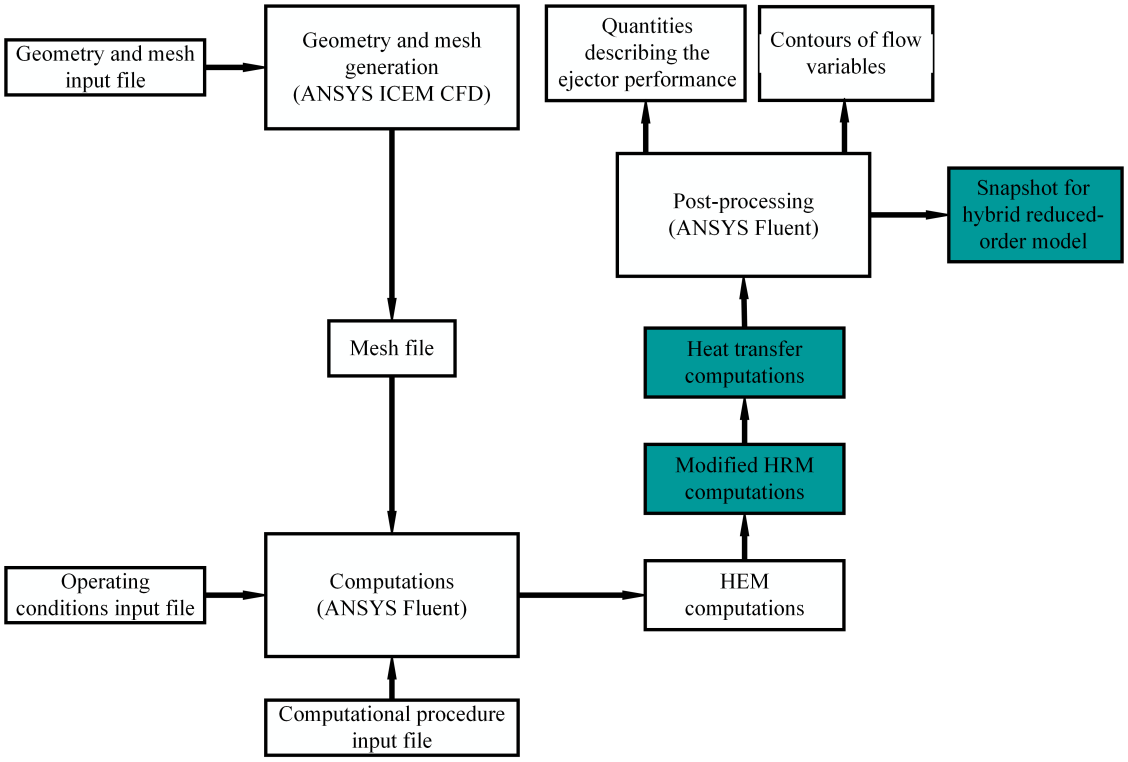

Figure 5: The simulation strategy using the *ejectorPL* platform adapted and modified from Palacz et al. (2017).

4.2. *Validation procedure of the R744 liquid ejector CFD model*

The ejector work can be described using MER and ejector efficiency definitions. MER is the ratio between the suction nozzle MFR and the motive nozzle MFR:

$$\chi = \frac{\dot{m}_{SN}}{\dot{m}_{MN}} \tag{1}$$

where χ is MER and $\dot{m}$ is the mass flow rate in kg·s^{-1} of the motive nozzle (MN) and the suction nozzle (SN). According to Elbel and Hrnjak (2008), the ejector efficiency can be defined as the ratio of the work rate of the recovered ejector expansion to the recovery potential of the maximum expansion work rate:

$$\eta_{ej} = \frac{\dot{W}_{rec}}{\dot{W}_{rec,max}} = \chi \cdot \frac{h(p_{out}, s_{SN}) - h(p_{SN}, s_{SN})}{h(p_{out}, s_{MN}) - h(p_{MN}, s_{MN})} \tag{2}$$

where η_{ej} is the ejector efficiency, h is the specific enthalpy in J·kg^{-1}, $\dot{W}$ is the expansion work rate in W, s is the specific entropy in J·(kg^{-1}·K^{-1}) and p is the pressure in Pa.

In this paper, MFRs of investigated liquid ejectors given by the CFD model and the hybrid ROM were compared with the experimental data to define application range of each model. The discrepancies of both numerical approaches were calculated as the relative error formulated in the following form:

$$\delta_i = 1 - \frac{\dot{m}_{CFD/hROM}}{\dot{m}_{exp}} \cdot 100\% \tag{3}$$

where δ_i is the relative error of the motive nozzle mass flow rate, the suction nozzle mass flow rate, or entrainment ratio obtained by either the CFD model or the hybrid ROM with respect to the experimental data.

The CFD model results of the validation procedure along with the experimental data for liquid ejector LEJ1 are listed in Table 6. The relative difference of the MN MFR confirmed high accuracy of the CFD model at transcritical conditions. A very good agreement of MN MFR within ±5% was obtained for almost all operating points for MN conditions above the critical point. The CFD model slightly overestimated the MN MFR above 80 bar for L1_1, L1_7 and L1_9. The unsatisfactory MN MFR prediction above ±10% was reached for L1_2 as the results of the very high MN pressure over 95 bar and high MN temperature close to 312 K. The SN MFR accuracy was within ±10% for most validated points at transcritical conditions except L1_9 and L1_11. The overestimation of the SN MFR above the defined threshold at the aforementioned points was affected by the very high pressure lift above 10 bar. The MER discrepancy above ±10% was obtained for L1_4, L1_9, and L1_11 due to the overestimation of the SN MFR.

The CFD results for operating conditions close to the critical point (from L1_13 to L1_18) satisfactorily predicted MN MFR, SN MFR and MER within ±10%. In the subcritical operating regime, the MN MFR accuracy within ±10% was obtained for most of the validated points. The modified HRM CFD model estimated SN MFR and MER in a good agreement to the operating conditions below critical conditions. An unsatisfactory prediction of the MN MFR above 10% was reached for L1_20, L1_21, L1_24 defined for the MN pressure above 60 bar caused by the underestimation of the metastable motive nozzle flow, especially close to the saturation line. At the MN pressure below 55 bar, the modified HRM CFD model obtained significant underestimation of the MN MFR above 10%. Therefore, an acceptable accuracy within ±10% of the MN MFR was obtained for a similar application range defined by Haida et al. (2018c). The acceptable accuracy of the SN MFR at the subcritical conditions was reached for most of the validated points except L1_22 and L1_31. As a result of the high MN MFR and SN MFR discrepancies, the MER accuracy above ±10% was reached for L1_21, L1_22, L1_25, L1_30, and L1_31 at the subcritical conditions. However, the acceptable accuracy of the MER for most of the validated points above 55 bar allows for the evaluation of the liquid ejector performance at different pressure lift.

Table 7 shows a comparison between the CFD results and the experimental data for the liquid ejector LEJ2 at different operating conditions. The CFD model MN MFR achieved a high accuracy within ±10% at transcritical conditions for all the evaluated points. Moreover, SN MFR and MER satisfactorily predicted above the critical point except L2_1 and L2_2. The unsatisfactory underestimation of the SN MFR and MER at the aforementioned operating points was affected by slightly overestimated MN MFR and small pressure lift of 3 bar for L2_1.

The CFD results for operating conditions below the critical point satisfactorily predicted the MN and SN MFRs and MER within ±10% for the MN pressures above 60 bar. Moreover, the SN MFR accuracy was within the specified threshold for the operating points from L2_12 to L2_17 as the results of accurate prediction of the motive flow. Finally, the high accuracy of both flows caused the similar accuracy of MER within ±10%. An unsatisfactory MN MFR prediction above 10% was reached for the operating points from L2_18 to L2_22 due to the underestimation of the metastable motive flow by the modified CFD model. High underestimation of the motive flow resulted in a high inaccuracy in the SN MFR prediction up to 30% for L2_22 as well as MER for L2_18 and L2_20. Hence, the modified HRM CFD model of the R744 liquid ejector LEJ2 estimated the MFR of both nozzles with satisfactory prediction at transcritical and subcritical conditions above 60 bar.

4.3. Metastability flow inside the liquid ejector

The numerical investigation of the R744 liquid ejector performed by Haida et al. (2016b) indicated high inaccuracy of the homogeneous equilibrium model either in subcritical as well as in the transcritical conditions. The unsatisfactory prediction of both mass flow rates was caused by the metastability of the motive flow expanded in

Table 6: The set of the modified HRM CFD results of the R744 liquid ejector LEJ1 compared with experimental data from Table 4.

OC	CFD model results				
	$\dot{m}_{MN}$ kg·min^{-1}	$\dot{m}_{SN}$ kg·min^{-1}	$\delta_{\dot{m}_{MN}}$ %	$\delta_{\dot{m}_{SN}}$ %	δ_{χ} %
L1_1	3.28	2.37	-8.9	-0.9	7.4
L1_2	3.30	2.56	-10.5	-7.8	2.5
L1_3	3.26	1.78	2.7	5.9	3.2
L1_4	3.06	2.79	1.5	-8.8	-10.5
L1_5	3.27	2.35	0.7	-7.1	-7.8
L1_6	3.06	1.93	3.6	0.5	-3.2
L1_7	3.16	2.95	-0.1	-4.2	-4.1
L1_8	3.10	1.73	3.4	4.1	0.7
L1_9	3.31	2.26	-0.2	-10.4	-10.2
L1_10	3.10	2.35	0.5	-2.2	-2.7
L1_11	2.93	1.59	1.1	-14.5	-15.8
L1_12	5.68	2.54	8.4	6.4	-2.2
L1_13	3.33	2.30	1.4	-3.2	-4.7
L1_14	3.15	2.28	2.7	-6.0	-8.9
L1_15	3.19	2.76	1.9	0.3	-1.6
L1_16	2.72	1.59	9.9	7.4	-2.7
L1_17	3.03	2.65	5.0	1.2	-4.0
L1_18	2.75	2.34	8.2	7.6	-0.7
L1_19	5.19	2.40	7.1	5.4	-1.8
L1_20	5.05	2.48	11.1	7.0	-4.5
L1_21	2.63	1.49	17.4	0.7	-20.2
L1_22	5.06	3.40	8.0	-31.1	-42.4
L1_23	3.41	0.34	9.7	2.1	-8.4
L1_24	3.01	2.15	10.3	1.8	-9.5
L1_25	3.07	2.71	8.9	-2.8	-12.8
L1_26	3.04	1.97	8.1	9.2	1.1
L1_27	3.27	1.54	5.5	-0.2	-6.0
L1_28	3.18	0.51	6.6	8.0	1.5
L1_29	3.04	0.46	8.1	2.2	-6.4
L1_30	3.09	0.35	13.8	-2.3	-18.8
L1_31	2.88	1.76	24.8	13.6	-15.0

the converging-diverging nozzle and the suction stream slightly expanded in the pre-mixer chamber. Therefore, the modified homogeneous relaxation model allows for the improvement of the accuracy of the CFD model, which was presented in Section 4.2.

The metastability of the motive and suction flows strongly related to the flow parameters such as the density, pressure, specific enthalpy, and vapour quality. Figure 6 presents the contour plot of the non-dimensional parameter called void fraction that describing the relation between the instantaneous quality and the local density. The analysis was done for liquid ejector LEJ2 at the subcritical operating conditions L2_12 and L2_13 defined for different subcooling degree at the motive nozzle pressure of approximately 70 bar. The rapid increase of the void fraction at the motive nozzle throat was observed at L2_12 as the result of the motive nozzle conditions close to the saturation line and a deeper expansion into the two-phase region. Therefore, the metastability effect stronger influenced the motive nozzle mass flow rate due to the evaporation delay around the motive nozzle throat. At

Table 7: The set of the modified HRM CFD results of the R744 liquid ejector LEJ2 compared with experimental data from Table 5.

OC	CFD model results				
	$\dot{m}_{MN}$ kg·min^{-1}	$\dot{m}_{SN}$ kg·min^{-1}	$\delta_{\dot{m}_{MN}}$ %	$\delta_{\dot{m}_{SN}}$ %	δ_{χ} %
L2_1	5.73	4.80	-0.4	11.4	11.7
L2_2	6.10	4.67	-5.2	12.8	17.1
L2_3	5.92	4.22	-1.8	6.2	7.8
L2_4	6.03	4.53	-5.9	1.8	7.2
L2_5	8.28	2.25	0.4	2.9	2.5
L2_6	8.07	2.27	0.1	6.1	6.7
L2_7	5.65	3.09	6.1	6.0	-0.1
L2_8	8.70	1.69	3.8	4.2	0.4
L2_9	8.69	1.53	2.4	7.2	4.9
L2_10	5.45	4.26	8.6	9.9	1.4
L2_11	5.24	4.78	8.5	0.4	-8.9
L2_12	6.04	3.36	5.3	1.2	-4.4
L2_13	8.90	1.46	1.6	1.5	-0.1
L2_14	6.34	3.05	3.2	1.8	-1.4
L2_15	5.81	4.00	7.7	1.3	-6.9
L2_16	6.14	2.06	5.3	5.4	0.0
L2_17	6.12	2.53	9.1	8.7	-0.5
L2_18	7.31	4.08	25.1	12.0	-17.5
L2_19	6.00	2.78	18.9	14.7	-5.1
L2_20	5.88	1.34	26.3	17.8	-11.6
L2_21	6.47	2.96	18.8	21.6	3.4
L2_22	5.85	2.98	24.0	29.4	7.1

L2_13, the motive nozzle flow was expanded close to the saturation line and the void fraction increased right after the motive nozzle throat in the pre-mixing chamber. Moreover, a slightly increase of the void fraction was observed in the suction nozzle and close to the wall in the mixing section for both operating conditions. Hence, the delay of the evaporation by consideration of the metastability effect influenced the entrainment possibility of the motive flow and the suction nozzle mass flow rate. The void fraction was above 0.5 along the mixing section and at the beginning of the diffuser as the effect of the momentum transfer between both streams. In addition, the lower values of the void fraction in the mixer and at the beginning of the diffuser were observed at L2_13 when compared to L2_12 due to the differences of the motive nozzle conditions, expansion process of the motive stream and higher MER corresponded to the lower pressure lift at L2_12.

Figure 7 shows the pressure distribution along the liquid ejector axis together with the relaxation time at the operating conditions L2_13. Moreover, the saturation pressure was included to define the beginning of the two-phase flow. The pressure rapidly dropped and the two-phase region appeared close to the nozzle throat. In addition, the highest value of the relaxation time approximately 3.5 seconds appeared at the beginning of the two-phase region and then the metastable effect decreased. The high relaxation of the evaporation in the motive nozzle caused an increase of the motive nozzle mass flow rate as the result of higher density. In the mixing section, the pressure increased up to approximately 30 bar and it stabilised along the mixing section. The similar behaviour was observed for the relaxation time in the mixing section. Hence, the mixing process was also influenced by the metastability of the motive and suction streams.

The proposed CFD numerical model allows the R744 liquid ejectors to be accurately simulated in a very wide operating regime. However, the implementation of the aforementioned approach into a dynamic simulation of a

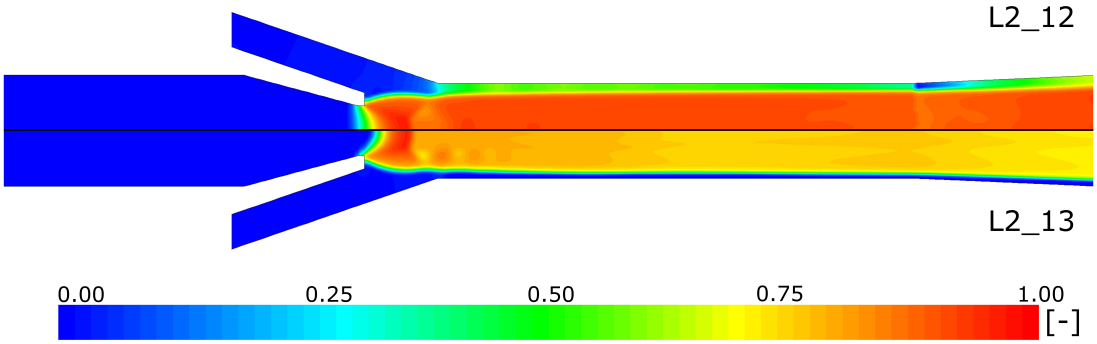

Figure 6: The contour plot of the void fraction parameter describing metastable flow at the operating conditions L2_12 and L2_13.

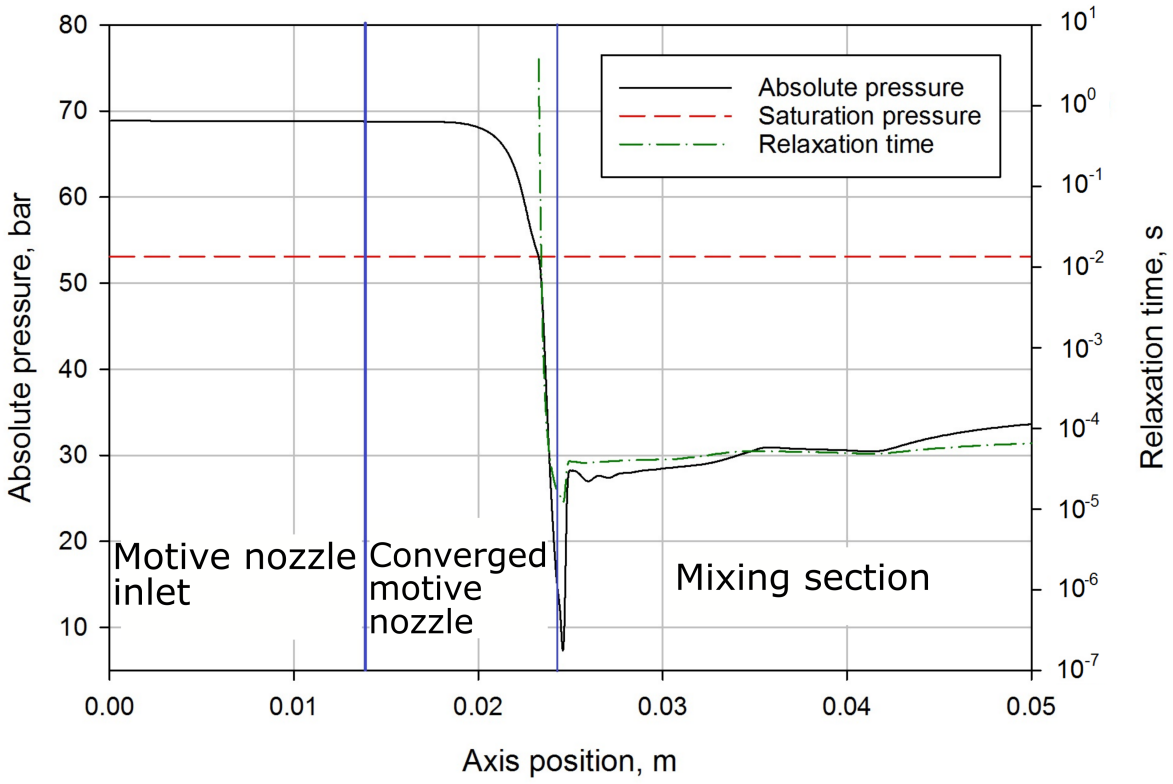

Figure 7: The pressure distribution and the relaxation time along the liquid ejector axis at the operating conditions L2_13.

CO_2 HVAC&R supermarket system is impossible to perform an ejector calculation due to the single case computational time. Therefore, the fast and accurate hybrid ROM was used in the present investigation.

5. Hybrid ROM

The main aim of the developed low-order model is to continously calculate the ejector mass flow rates at arbitrary pressure-based operating conditions. Haida et al. (2018a) already described reduced-order approach.For sake of completeness, this is repeated here as follows: "The POD-RBF apporach allows fast computation due to the considered input data in the POD basis defined as a single vector called snapshot". The snapshot generated from the CFD results was prepared in manner similar to the snapshot based on the experimental data that used both inputs in the hybrid ROM basis. A single snapshot was defined as the set of MN and SN MFRs for single boundary conditions within the defined operating regime. An additional details about the POD-RBF mathematical approach can be found in Haida et al. (2018a).

Each hybrid ROM was generated based on the selected CFD results combined with all the experimental data obtained during test campaign. Therefore, the total number of CFD points together with operating conditions had to be defined to cover the operational envelope presented in Figure 2. The number of CFD points was strongly related to the combination of the motive nozzle, suction nozzle and outlet conditions. Based on the previous investigation performed on the R744 vapour ejectors by Haida et al. (2018a), the CFD points were defined using defined pressure and temperature steps in the following order:

- motive nozzle pressure: 2 bar,
- motive nozzle temperature: 1 K,
- suction nozzle pressure: 2 bar,
- outlet pressure: 2 bar.

Based on the specified operating regime and aforementioned steps between points, the total number of the CFD points was of 1767 for each liquid ejector generated using an automatic tool *ejectorPL*.

The developed hybrid ROM of the R744 liquid ejector was used to evaluate the ejector performance at arbitrary operating conditions within the envelope discussed in Section 4. Hence, the validation procedure was performed to define the accuracy of the hybrid ROM for both investigated ejectors. Figure 8 presents the accuracy of the MN and SN MFRs of each liquid ejector hybrid ROM. Similar operating points were used to define the accuracy of the CFD model and were selected for the validation. A hybrid ROM was built based on all CFD results and only 50% of randomly-selected experimental data. Only 50% of the experimental data was selected to evaluate the accuracy improvement of the low-order model by integration of the CFD results with the chosen experimental data.

The MN MFR accuracy of the hybrid ROM for LEJ1 is shown in Figure 8(a) on a pressure-specific enthalpy diagram. The accuracy was within ±5% for most of the investigated points, especially in the subcritical region and close to the critical temperature. Therefore, the hybrid combination of the experimental data and the CFD results improves the low-order prediction of the MN MFR compared to the CFD results. The discrepancy of the MN MFR above ±5% was reached for an MN pressure of approximately 90 bar and at high degrees of sub-cooling. The hybrid ROM LEJ1 obtained a similarly high accuracy for SN MFR within ±5% for most of the validated points, which is shown in Figure 8(b). The lowest accuracy within ±20% was reached for a very low pressure lift of 3 bar at an SN pressure of approximately 26 bar and for a pressure lift of approximately 9 bar for SN pressure near 30 bar. It can be concluded that the hybrid ROM best predicted the MFR of both nozzles for pressure lifts below 9 bar and at the refrigeration application conditions. An increase in the subcooling degree increased the model discrepancy, and similar trends were also observed for the CFD in Section 4.2.

The hybrid ROM of LEJ2 obtained similarly good agreement of the MN and SN MFRs when compared to the hybrid ROM of LEJ1. The MN MFR had an accuracy within ±5% of the hybrid ROM LEJ2 presented in Figure 8(c) for most of the investigated points at subcritical conditions, close to the critical point, and in transcritical conditions. A high discrepancy of the MN MFR within ±15% was obtained at MN pressures above 90 bar and at MN temperatures higher than the critical temperature. The SN MFR accuracy of the hybrid ROM LEJ2 was within

±5% for most of the validated points at different pressure lift and SN pressures, which is shown in Figure 8(d). However, the hybrid ROM of LEJ2 showed a high discrepancy of ±20% of the SN MFR for additional investigated operating conditions compared to the hybrid ROM of LEJ1. Therefore, increasing the measured experimental data of the hybrid ROM improved the accuracy of the low-order model to evaluate the performance mapping of the liquid ejectors with a high accuracy.

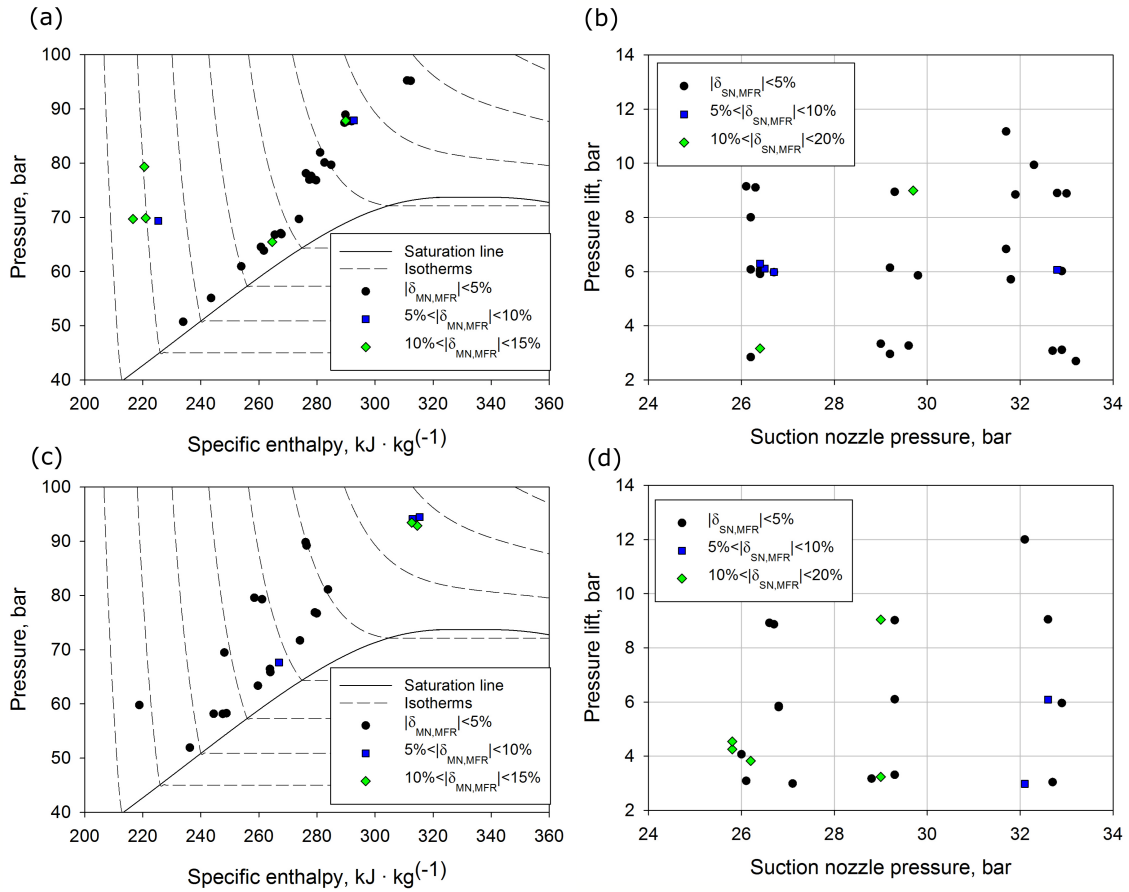

Figure 8: The accuracy of the hybrid ROM based on the CFD model and 50% of experimental data of both liquid ejectors: (a) MN conditions at the R744 p-h diagram of LEJ1; (b) the pressure lift in terms of the SN pressure of LEJ1; (c) MN conditions at the R744 p-h diagram of LEJ2; (b) the pressure lift in terms of the SN pressure of LEJ2.

Table 8 presents the overall comparison between the hybrid ROM that considered 50% of randomly-selected experimental data to the model base and the hybrid ROM built based on the all CFD results and all experimental data. The accuracy of the MN and SN MFR was compared for both investigated liquid ejectors. The MN MFR prediction of the hybrid ROM with 50% of randomly-selected experimental data achieved an accuracy within ±5% for 77% for LEJ1 and 82% for LEJ2 of all considered validation points. Moreover, the SN MFR accuracy was within ±5% for approximately 80% of the investigated points for both hybrid ROMs. Including all experimental data to build the hybrid ROM improved the accuracies of the MN and SN MFRs for both liquid ejectors. Hence, the hybrid ROM obtained an accuracy within ±5% for all operating points selected for validation.

The validation procedure of the hybrid ROM liquid ejector confirmed the acceptable prediction of the MFR of both nozzles within the defined operating regime. Therefore, performance mapping can be performed to evaluate the work of each designed liquid ejector at different operating conditions appearing in the R744 integrated system.

Table 8: MN and SN MFR accuracy obtained from the hybrid ROM based on all CFD results and either 50% experimental data or 100% experimental data for all experimental points considered in the validation.

Input data	Accuracy range	LEJ 1		LEJ 2	
		MN	SN	MN	SN
CFD + 50% experimental data	$\|\delta_i\| < 5\%$	0.77	0.81	0.82	0.78
	$\|\delta_i\| > 5\%$	0.23	0.19	0.18	0.22
CFD + 100% experimental data	$\|\delta_i\| < 5\%$	1.00	1.00	1.00	1.00
	$\|\delta_i\| > 5\%$	0.00	0.00	0.00	0.00

6. Performance maps of the R744 liquid ejectors

The use of a liquid ejector in the R744 integrated supermarket system is related to the cooling capacity and the ambient conditions. Moreover, the generation of performance maps for each desgined liquid ejector allows definition of the specific performance region and behaviour similar for each ejector. Therefore, the map of the MN MFR at different MN conditions allowed the capacity of each ejector to be set to efficiently control the system, which is shown in Figure 9. The MN MFR maps of both ejectors were defined for different MN pressures and specific enthalpies within a defined operating regime. Moreover, SN conditions were defined for an overfed MT evaporation temperature of -4 °C according to Gullo et al. (2018b). The pressure lift was set to 4 bar for both investigated liquid ejectors, and a similar trend was observed for each ejector. The lowest MFR values were reached close to the critical point, and the MN MFR increased with the pressure and specific enthalpy. The highest MFR values were achieved at a MN pressure of 140 bar and MN specific enthalpy of approximately 240 kJ·kg^{-1}. The MN MFRs obtained by LEJ1 in Figure 9(a) were approximately two times smaller compared to MN MFRs of LEJ2 in Figure 9(b). The highest value of the MN MFR of LEJ2 was approximately 0.3 kg·s^{-1}, whereas the MN MFR of LEJ1 was approximately 0.15 kg·s^{-1}. In addition, the area of lowest MN MFRs was close to the saturation line and the critical point similar to results presented for LEJ1 in Figure 9(a). The same trend of the MN MFR increase was observed for LEJ2 during increase of the pressure and decrease of the specific enthalpy when compared to LEJ1 performance map. Hence, the work of the investigated liquid ejectors installed in the multi-ejector module can be controlled by properly setting the operating conditions and running the ejectors in either single or in parallel operating modes.

Figure 10 presents the effect of the SN saturated conditions on the MER of both liquid ejectors. The MN temperature was set to 40 °C, and the MN pressure was 102.4 bar to evaluate the performance of the liquid ejectors in a tropical climate zone (Purohit et al., 2018). The MN pressure was set according to an approximation function of the gas cooler pressure in the R744 multi-ejector system presented by Gullo et al. (2017). The investigation was conducted for two pressure lifts of 4 and 14 bar to evaluate the work of the investigated ejectors at different liquid receiver pressures. The MER of LEJ1 was higher for both defined pressure lifts compared to LEJ2 for SN pressures between 26 and 46 bar. However, the MER of LEJ1 dropped more significantly when the pressure lift increased, especially for high SN pressures. LEJ1 obtained a MER for a pressure lift of 4 bar of over 0.4 at an SN pressure of 26 bar up to below 1.6 and in the range from approximately 0.1 to over 1.0 for the pressure lift of 14 bar. Both liquid ejectors reached the maximum possible MER for high pressure lift close to an SN pressure of 45 bar. The MER of LEJ2 varied from approximately 0.1 to 1.2 for a pressure lift of 4 bar and from 0.1 to approximately 1.1 for a pressure lift of 14 bar.

According to the results shown in Figure 10, the investigated liquid ejectors showed lower performances under refrigeration conditions compared to AC conditions, which are strongly related to the energy performance of the R744 integrated system. Hence, identifying the maximum possible efficiency of an ejector at different ambient conditions and for both applications would control the R744 integrated supermarket system at the highest COP.

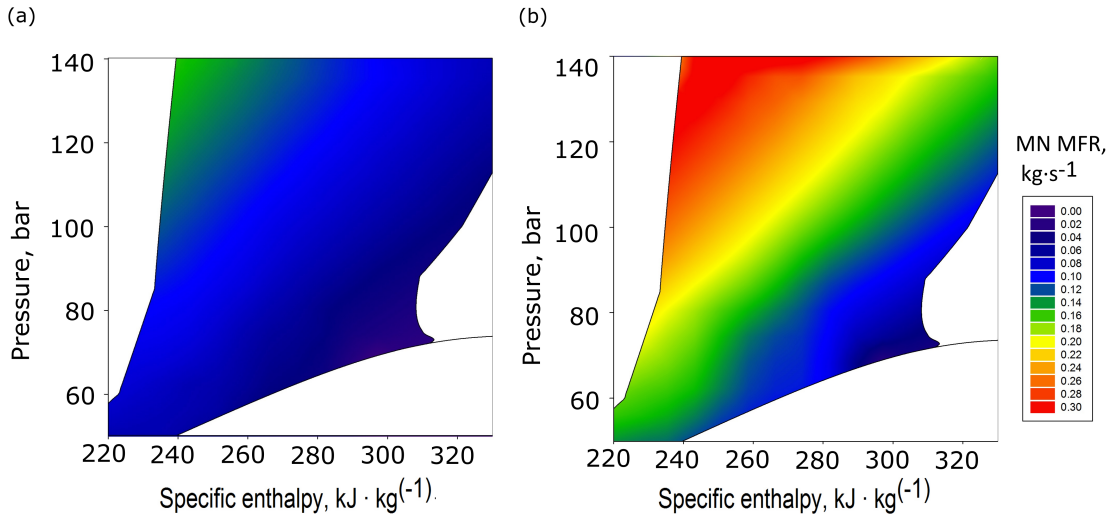

Figure 9: The motive nozzle mass flow rate maps of the investigated liquid ejectors at a MT evaporation temperature of -4 °C and a pressure lift of 4 bar: (a) LEJ1; (b) LEJ2.

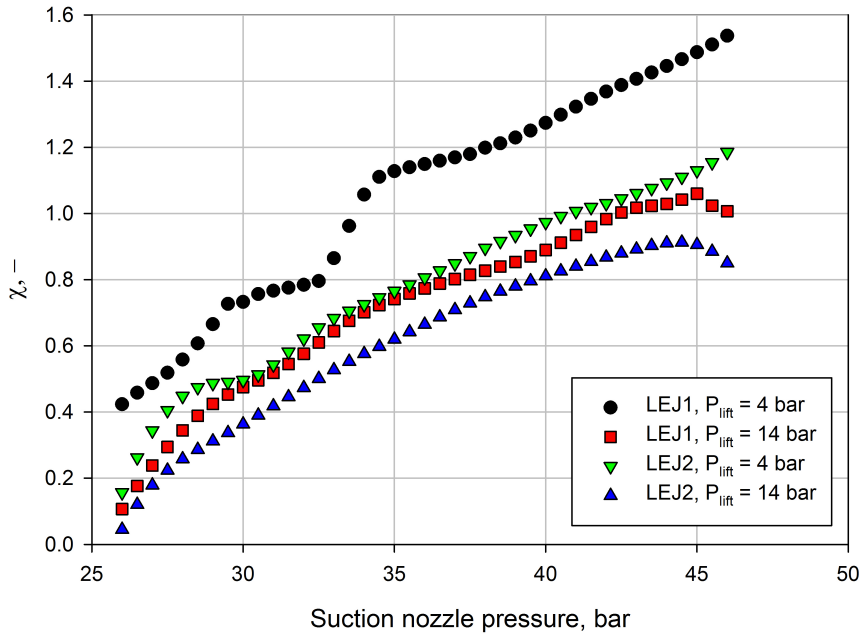

Figure 10: MER in terms of the suction nozzle pressure of both investigated liquid ejectors at an MN pressure of 102.4 bar and MN temperature of 40 °C.

7. Liquid ejectors performance maximisation

Integrating liquid ejectors and vapour ejectors with a R744 integrated system requires optimum control of the system to maintain the highest COP due to overfeeding the refrigeration evaporators and air-conditioning applications and expansion work recovery by using the ejectors. Hence, the investigated liquid ejectors installed

in the multi-ejector module should be operated at the highest efficiency. Moreover, the proper set of pressure lifts at different ambient conditions must be defined for the best liquid ejector performance.

Figure 11 presents the pressure lift and the maximum ejector efficiency in terms of different MN pressures of both liquid ejectors for refrigeration applications. The MN temperature was defined based on the correlations presented by Gullo et al. (2017) which are strongly related to ambient temperatures from approximately 14 °C for cold climates to 50 °C for tropical climates. A similar investigation was done for vapour ejectors installed in a multi-ejector module by Haida et al. (2018a). SN conditions were defined for an MT evaporation temperature of -6 °C. The pressure lift of LEJ1 presented in Figure 11(a) increased from 5 bar for MN pressure up to 11 bar for MN pressure below 84 bar. Moreover, the highest ejector efficiency was approximately 0.07 for an MN pressure of 78 bar and the increase in the ambient conditions caused the ejector efficiency to drop to approximately 0.015. The LEJ1 efficiency varied between 0.025 and 0.04 at subcritical conditions, and a similar ejector efficiency trend was shown by LEJ2 compared to LEJ1, as shown in Figure 11(b). However, the LEJ2 efficiency was slightly higher than the LEJ1 ejector efficiency at subcritical conditions, and a maximum value of approximately 0.09 was obtained for an MN pressure of 78 bar. Further increases in the ambient temperature caused a significant drop in the LEJ2 ejector efficiency, which reduced the performance compared to LEJ1. The pressure lift of LEJ2 increased from 5 bar to 11 bar at MN pressures below 82 bar, and a pressure lift of 10 bar was reached for MN pressures above 120 bar due to the very low SN MFR.

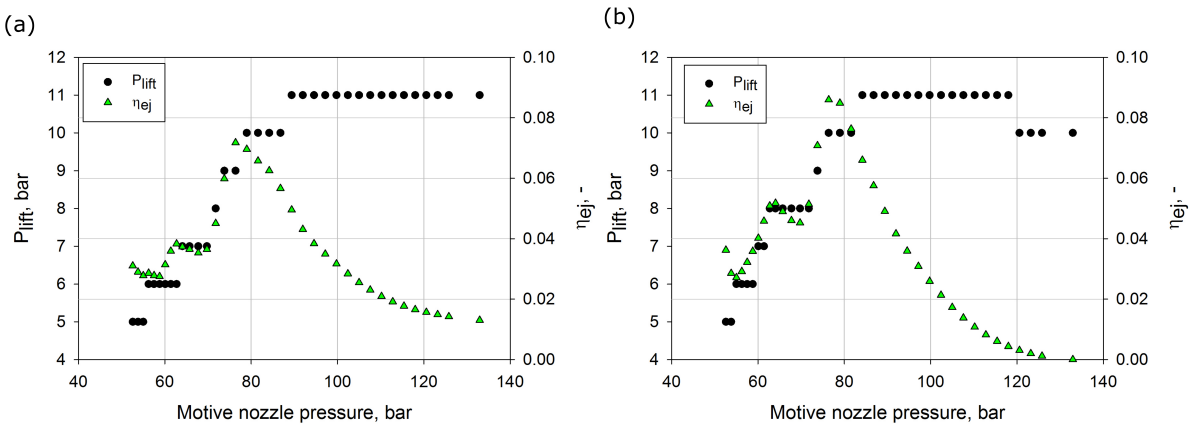

Figure 11: The pressure lift and the maximum ejector efficiency in terms of the different MN conditions of the investigated liquid ejectors at an MT evaporation temperature of -6 °C: (a) LEJ1; (b) LEJ2.

Similar to the investigation of the best liquid ejector performance for refrigeration, the pressure lift and maximum ejector efficiency in terms of the different MN conditions for air-conditioning are shown in Figure 12. The MN pressure was defined from 50 bar to 140 bar, and the MN temperature was defined according to the correlations presented by Gullo et al. (2017). Moreover, the SN conditions were defined for an air-conditioning evaporation temperature of 5 °C. A similar pressure lift trend was obtained by both liquid ejectors from approximately 3 bar at an MN pressure of 50 bar to 14 bar at an MN pressure above 110 bar. The LEJ1 efficiency ranged from approximately 0.03 to 0.04 for subcritical conditions, and a maximum efficiency of approximately 0.09 was reached for an MN pressure of 82 bar. Further increases in the MN pressure at transcritical conditions decreased the LEJ1 efficiency to below 0.04. The LEJ2 efficiency trend was similar to LEJ1, but the efficiency varied from approximately 0.05 to 0.07 in the subcritical region and a maximum efficiency of approximately 0.11 for an MN pressure of 79 bar. A decrease in ejector efficiency was obtained at MN pressures above 79 bar, and the lowest efficiency was less than 0.02 for an MN pressure of 140 bar.

Selecting the proper set of pressure lifts allows the best performance of liquid ejectors installed in the multi-ejector module to be maintained. Moreover, the high pressure lift values reduced the pressure ratio of the parallel compressor, which is strongly related to the system energy performance. Hence, the control strategy of the R744 integrated supermarket system equipped with liquid and vapour ejectors should dynamically operate the multi-

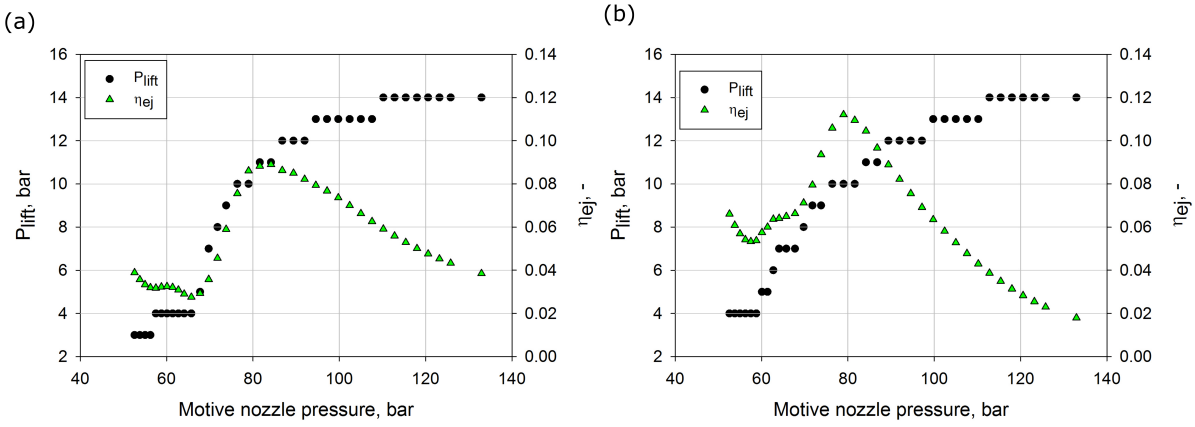

Figure 12: The pressure lift and the maximum ejector efficiency in terms of the different MN conditions of the investigated liquid ejectors at an air-conditioning evaporation temperature of 5 °C: (a) LEJ1; (b) LEJ2.

ejector work to achieve a continuously optimum COP. Moreover, the design of vapour and liquid ejectors should obtain the similar operation curves to maintain the optimum COP. However, that kind of investigation can be done only using advanced mathematical model of the vapour ejector and the liquid ejector implemented to the dynamic simulations of the R744 refrigeration system. Hence, the optimisation study of the R744 refrigeration system equipped with vapour and liquid ejectors must be performed based on the dynamic simulation with the implemented ROMs of the designed vapour and liquid ejectors.

8. Conclusions

A numerical investigation of liquid ejectors based on a CFD model and the hybrid reduced-order model was carried out. Performance mapping of two liquid ejectors installed in the multi-ejector module was presented at different applications appearing in the R744 integrated supermarket system. The liquid ejectors were designed to have an increased capacity in the binary order to cover the cooling demand in a supermarket system. Moreover, the pressure lift needed to obtain the best efficiency of each liquid ejector was investigated at different ambient conditions for refrigeration and air-conditioning applications.

The CFD model, together with the modified homogeneous relaxation two-phase fluid flow assumption of the liquid ejector, was used to build a hybrid reduced-order model. The validation procedure of the modified homogeneous relaxation CFD model confirmed the high accuracy of the motive nozzle and suction nozzle MFR predictions at subcritical conditions, close to the critical point, and at the transcritical conditions. A satisfactory prediction of the mass flow rates of both nozzles within ±10% was obtained for the motive nozzle pressure above approximately 60 bar, and similar results were obtained for both liquid ejectors. Therefore, the results given by the modified homogeneous relaxation CFD model, combined with the experimental data carried out at the R744 vapour compression test rig, allowed the development of a fast hybrid reduced-order model.

The validation performed for the hybrid reduced-order model indicated improved accuracy compared to the CFD model. The hybrid reduced-order model with only 50% randomly selected experimental data let to predict the motive nozzle and suction nozzle mass flow rates within ±5% at transcritical conditions and subcritical conditions. Moreover, using all experimental data improved the hybrid ROM accuracy within ±1% at all investigated operating points.

The performance mapping of the R744 liquid ejectors was accomplished by generating the motive nozzle mass flow rate maps together with the mass entrainment ratio at different suction nozzle conditions and pressure lifts. The motive nozzle mass flow rate map of each investigated ejector indicated the area of the lowest mass flow rate close to the critical point. A similar trend was observed in the motive nozzle mass flow rate increase for both liquid ejectors. The highest values of the motive nozzle mass flow rate were reached at a motive nozzle pressure of 140

bar and a very low motive nozzle temperature that corresponded to the low specific enthalpy. The motive nozzle mass flow rate of LEJ1 varied in the range from 0.01 to 0.15 kg·s^{-1} and motive nozzle mass flow rate of LEJ2 was two times larger than LEJ1 and less than approximately 0.3 kg·s^{-1}. The mass entrainment ratio increased during increase of the suction nozzle pressure and at low pressure lifts and air-conditioning conditions, this parameter was above 1.0. However, increasing the pressure lift indicated the local maximum of the mass entrainment ratio, and further increases in the suction nozzle pressure decreased the mass entrainment ratio. Hence, liquid ejectors should be controlled based on the proper set of pressure lifts at different ambient conditions to maximise the liquid flow recirculation from the evaporator and to reduce the compression ratio in the parallel compressors.

Performance maximisation was investigated for both liquid ejectors based on identification of the maximum ejector efficiency by changing the pressure lift. The investigation was performed at different ambient conditions from cold climate zones to tropical climate zones. The suction nozzle conditions were defined for flooded medium temperature evaporator at the refrigeration application and flooded conditions at the air-conditioning evaporator. The ejector efficiency varied between 0.3 and 0.8 for LEJ1 and between 0.0 and 0.9 for LEJ2 at the refrigeration application. The pressure lift increased in the subcritical region from 5 bar at the motive nozzle pressure of 50 bar and reached stable pressure lift of 11 bar for the motive nozzle pressure above 80 bar for both investigated ejectors. The higher efficiency drop was observed for LEJ2 at the motive nozzle pressure above 100 bar and LEJ1 was utilised more efficiently at the tropical conditions. Similar pressure lift and ejector efficiency trends were observed by each liquid ejector in the air-conditioning application. A maximum pressure lift of 14 bar was obtained at the motive nozzle pressure above 120 bar, and the highest value of the ejector efficiency was of 0.09 for LEJ1 and above 0.11 for LEJ2. Therefore, the liquid ejectors indicated improved performance for air-conditioning compared to refrigeration.

Efficient control of the liquid ejectors work installed in the multi-ejector module allowed for the best energy performance of the R744 integrated supermarket system. Moreover, the liquid ejector operation should be adapted to a parallel work with the vapour ejectors to achieve a high mass entrainment ratio for the liquid flow recirculation at the optimum pressure lift values. The integration of the liquid and vapour ejectors requires optimisation of the working conditions, especially the pressure lift for the optimum COP. The possibility to maintain a high value of the pressure lift at transcritical conditions influenced the energy power consumption at the parallel compressors due to the pressure ratio reduction together with the increase in the evaporation temperature by flooding the evaporators. Hence, the dynamic simulation of the R744 multi-ejector integrated supermarket system combined with the optimisation procedure for the energy performance maximisation has to be done based on the developed reduced-order models of designed ejectors under subcritical and transcritical conditions. The aforementioned investigation allows for the determination of the efficient operation of the refrigeration system equipped with the liquid and vapour ejectors for different climate zones.

9. Acknowledgement

The authors gratefully acknowledge the financial support of the Research Council of Norway through project No. 244009/E20. The work of MH was also supported by the Rector's research grant No. 08/060/RGJ18/0157 provided by SUT. Moreover, the work of JS and JB was also supported by SUT research grants No. 08/060/BK_18/0181 and 08/060/RGJ18/0158.

References

Krzysztof Banasiak, Armin Hafner, Ekaterini E. Kriezi, Kenneth B. Madsen, Michael Birkelund, Kristian Fredslund, and Rickard Olsson. Development and performance mapping of a multi-ejector expansion work recovery pack for R744 vapour compression units. *International Journal of Refrigeration*, 57:265–276, 2015. ISSN 0140-7007. doi: http://dx.doi.org/10.1016/j.ijrefrig.2015.05.016.

Stefan Elbel and Pega Hrnjak. Experimental validation of a prototype ejector designed to reduce throttling losses encountered in transcritical R744 system operation. *International Journal of Refrigeration-Revue Internationale Du Froid*, 31(3):411–422, 2008. ISSN 0140-7007. doi: DOI10.1016/j.ijrefrig.2007.07.013.

European Parliament and Council of EU. Regulation (EU) no 517/2014 of the european parliament and of the council of 16 april 2014 on fluorinated greenhouse gases and repealing regulation (EC) no 842/2006 text with EEA relevance. 2014.

Paride Gullo, Armin Hafner, and Giovanni Cortella. Multi-ejector R744 booster refrigerating plant and air conditioning system integration – a theoretical evaluation of energy benefits for supermarket applications. *International Journal of Refrigeration*, 75:164– 176, 2017. ISSN 0140-7007. doi: http://dx.doi.org/10.1016/j.ijrefrig.2016.12.009.

Paride Gullo, Armin Hafner, and Krzysztof Banasiak. Transcritical r744 refrigeration systems for supermarket applications: Current status and future perspectives. *International Journal of Refrigeration*, 93:269 – 310, 2018a. ISSN 0140-7007. doi: https://doi.org/10.1016/j.ijrefrig.2018.07.001.

Paride Gullo, Konstantinos M. Tsamos, Armin Hafner, Krzysztof Banasiak, Yunting T. Ge, and Savvas A. Tassou. Crossing co2 equator with the aid of multi-ejector concept: A comprehensive energy and environmental comparative study. *Energy*, 164:236 – 263, 2018b. ISSN 0360-5442. doi: https://doi.org/10.1016/j.energy.2018.08.205.

Armin Hafner, Sven Forsterling, and Krzysztof Banasiak. Multi-ejector concept for R-744 supermarket refrigeration. *International Journal of Refrigeration-Revue Internationale Du Froid*, 43:1–13, 2014. ISSN 0140-7007. doi: DOI10.1016/j.ijrefrig.2013.10.015.

Michal Haida, Krzysztof Banasiak, Jacek Smolka, Armin Hafner, and Trygve M. Eikevik. Experimental analysis of the R744 vapour compression rack equipped with the multi-ejector expansion work recovery module. *International Journal of Refrigeration*, 64:93–107, 2016a. ISSN 01407007. doi: 10.1016/j.ijrefrig.2016.01.017.

Michal Haida, Jacek Smolka, Michal Palacz, Jakub Bodys, Andrzej J. Nowak, Zbigniew Bulinski, Adam Fic, Armin Hafner, and Krzysztof Banasiak. Numerical investigation of an R744 liquid ejector for supermarket refrigeration systems. *Thermal Science*, 20(4):1259–1269, 2016b. ISSN 1742-6596.

Michal Haida, Jacek Smolka, Armin Hafner, Ziemowit Ostrowski, Michał Palacz, Kenneth B. Madsen, Sven Försterling, Andrzej J. Nowak, and Krzysztof Banasiak. Performance mapping of the r744 ejectors for refrigeration and air conditioning supermarket application: A hybrid reduced-order model. *Energy*, 153:933 – 948, 2018a. ISSN 0360-5442. doi: https://doi.org/10.1016/j.energy.2018.04.088.

Michal Haida, Jacek Smolka, Armin Hafner, Ziemowit Ostrowski, Michal Palacz, Andrzej J. Nowak, and Krzysztof Banasiak. System model derivation of the CO_2 two-phase ejector based on the cfd-based reduced-order model. *Energy*, 144:941 – 956, 2018b. ISSN 0360-5442. doi: https://doi.org/10.1016/j.energy.2017.12.055.

Michal Haida, Jacek Smolka, Armin Hafner, Michal Palacz, Krzysztof Banasiak, and Andrzej J. Nowak. Modified homogeneous relaxation model for the R744 trans-critical flow in a two-phase ejector. *International Journal of Refrigeration*, 85:314 – 333, 2018c. ISSN 0140-7007.

A.R. Ismagilov, E.K. Spiridonov, and O.V. Belkina. Liquid jet ejector efficiency improvement. *Procedia Engineering*, 206:99 – 106, 2017. ISSN 1877-7058. doi: https://doi.org/10.1016/j.proeng.2017.10.444. International Conference on Industrial Engineering, ICIE 2017.

A.A. Kornhauser. The use of an ejector as a refrigerant expander. In *International Refrigeration and Air Conditioning Conference*, pages 1–11, The address of the publisher, 1990. Purdue University, Purdue ePubs. An optional note.

Neal Lawrence and Stefan Elbel. Numerical investigation of the effect of microchannel evaporator design and operation on the improvement potential of ejector refrigeration cycles. *Energy*, 164:21 – 34, 2018. ISSN 0360-5442. doi: https://doi.org/10.1016/j.energy.2018.08.179.

Silvia Minetto, Riccardo Brignoli, Claudio Zilio, and Sergio Marinetti. Experimental analysis of a new method for overfeeding multiple evaporators in refrigeration systems. *International Journal of Refrigeration*, 38:1 – 9, 2014. ISSN 0140-7007. doi: https://doi.org/10.1016/j.ijrefrig.2013.09.044.

Michal Palacz, Jacek Smolka, Adam Fic, Zbigniew Bulinski, Andrzej J. Nowak, Krzysztof Banasiak, and Armin Hafner. Application range of the hem approach for co2 expansion inside two-phase ejectors for supermarket refrigeration systems. *International Journal of Refrigeration*, 59:251 – 258, 2015. ISSN 0140-7007.

Michal Palacz, Jacek Smolka, Andrzej J. Nowak, Krzysztof Banasiak, and Armin Hafner. Shape optimisation of a two-phase ejector for CO_2 refrigeration systems. *International Journal of Refrigeration*, 74:210–221, 2017. ISSN 0140-7007. doi: http://dx.doi.org/10.1016/j.ijrefrig.2016.10.013.

Ángel A. Pardiñas, Armin Hafner, and Krzysztof Banasiak. Novel integrated co2 vapour compression racks for supermarkets. thermodynamic analysis of possible system configurations and influence of operational conditions. *Applied Thermal Engineering*, 131:1008 – 1025, 2018. ISSN 1359-4311. doi: https://doi.org/10.1016/j.applthermaleng.2017.12.015.

Nilesh Purohit, Vishaldeep Sharma, Samer Sawalha, Brian Fricke, Rodrigo Llopis, and Mani Sankar Dasgupta. Integrated supermarket refrigeration for very high ambient temperature. *Energy*, 165:572 – 590, 2018. ISSN 0360-5442. doi: https://doi.org/10.1016/j.energy.2018.09.097.

V. Sharma, B. Fricke, and P. Bansal. Comparative analysis of various CO_2 configurations in supermarket refrigeration systems. *International Journal of Refrigeration-Revue Internationale Du Froid*, 46:86–99, 2014. ISSN 0140-7007. doi: DOI10.1016/j.ijrefrig.2014.07.001.

Jacek Smolka, Zbigniew Bulinski, Adam Fic, Andrzej J. Nowak, Krzysztof Banasiak, and Armin Hafner. A computational model of a transcritical R744 ejector based on a homogeneous real fluid approach. *Applied Mathematical Modelling*, 37(3):1208–1224, 2013. ISSN 0307-904X. doi: http://dx.doi.org/10.1016/j.apm.2012.03.044.

D. Sooben, N. Purohit, R. Mohee, F. Meunier, and M. S. Dasgupta. R744 refrigeration as an alternative for the supermarket sector in small tropical island developing states: The case of mauritius. *International Journal of Refrigeration*, 2019. ISSN 0140-7007. doi: https://doi.org/10.1016/j.ijrefrig.2019.03.034.

K. Sumeru, H. Nasution, and F. N. Ani. A review on two-phase ejector as an expansion device in vapor compression refrigeration cycle. *Renewable and Sustainable Energy Reviews*, 16(7):4927–4937, 2012. ISSN 1364-0321. doi: DOI10.1016/j.rser.2012.04.058.

United Nations. *Briefing Note on Ratification of the Kigali Amendment*. UN Environment Ozone Secretariat, 2017.

Q. Zaheer and J. Masud. Visualization of flow field of a liquid ejector pump using embedded les methodology. *Journal of Visualization*, 20(4):777–788, Nov 2017. ISSN 1875-8975. doi: 10.1007/s12650-017-0429-3.